



Influence of the atmospheric plasma spraying parameters on the coating structure and the deposition efficiency of silicon powder

Kirsten Bobzin¹ · Lidong Zhao¹ · Hendrik Heinemann¹ · Elisa Burbaum¹

Received: 23 May 2022 / Accepted: 20 August 2022 / Published online: 23 September 2022
© The Author(s) 2022

Abstract

Silicon coatings are usually produced by atmospheric plasma spraying (APS) and used as bond coats in environmental barrier coatings. The deposition efficiency (DE) of silicon powders is generally at a low level in APS processes. The reasons for the low DE values of silicon powders have not been sufficiently investigated in the literature. The aim of this study was to investigate in detail the influence of process parameters on the coating structure and deposition efficiency of a silicon powder processed with APS. A silicon powder with a size distribution of $f = -53 + 15 \mu\text{m}$ was sprayed using a three-cathode plasma generator to produce coatings. The parameters such as plasma gas type, plasma gas flow rate and current intensity were varied widely. Accordingly, the power of the plasma generator increased from $P = 19.4$ to 51.3 kW, which allowed different melting and evaporation degrees of the powder. Particle velocities and temperatures were measured using a particle diagnostic method. The coatings were investigated in terms of their surfaces and structures using electron scanning microscopy (SEM). The porosities of the coatings were measured using an image analysis system. The deposition efficiency of the processed powder was determined. The results show that the used parameters led to high particle velocities in a range of about $v_p = 270\text{--}360$ m/s. High particle temperatures of $T_p = 2,650\text{--}3,390$ °C were determined. The coating porosity varied from $\Phi = 2\%$ to $\Phi = 15\%$. The porosity value of $\Phi = 2\%$ is significantly lower than the values reported in the literature. The deposition efficiency of the powder changed from $\text{DE} = 1.5\%$ to $\text{DE} = 28\%$. The value of $\text{DE} = 28\%$ is about 40% higher than the values reported in the literature. The strong grit-blasting effect was the main reason for the lowest DE value of $\text{DE} = 1.5\%$. The strong evaporation effect was the main reason for the second lowest DE value of $\text{DE} = 11.1\%$. Numerous melted particles and semi-melted particles splashed upon impact with the substrate, resulting in silicon melt loss. In addition, solid cores of semi-molten particles could bounce off, which also resulted in silicon loss. Splashing and bouncing were the main factors affecting DE for the parameter sets with DE values ranging from 18.7% to 28%.

Keywords Silicon · Atmospheric plasma spraying · Deposition efficiency · Structure · Particle temperature · Particle velocity

1 Introduction

Environmental barrier coatings (EBCs) protect components of ceramic matrix composites (CMC) like SiC-fiber-reinforced SiC composites in modern aeroplane engines against water vapor-induced corrosion at high temperatures, as reported by Lee et al. in a review paper on EBCs

[1]. Current EBCs are multilayer systems. A silicon bond coat provides the desirable oxidation resistance and the needed adherence to the substrate, while the rare earth silicate top coat obstructs the recession by water vapor. A middle layer of mullite provides the required transition of the coefficient of thermal expansion (CTE) between the top coat and the bond coat.

APS is widely used to produce coatings for various applications. The temperature and velocity of plasma gas stream can be largely varied by adjusting plasma gas type, plasma gas flow rate and current. In combination with setting carrier gas flow rate, powder feed rate and stand-off distance, particle temperatures and velocities can be adjusted to achieve

✉ Lidong Zhao
zhao@iot.rwth-aachen.de

¹ Surface Engineering Institute, RWTH Aachen University, Kackertstr. 15, 52072 Aachen, Germany

the desired coating structures and properties with respect to the requirements of applications. APS is used to process a wide range of spray feedstock materials such as high melting ceramics [2, 3], carbide-based materials [4, 5] and metallic materials [6–8]. Gd_2O_3 - Yb_2O_3 co-doped YSZ highly porous coatings of more than $\Phi = 30\%$ were deposited for thermal barrier application in [2], while dense alumina-based coatings of less than $\Phi = 2\%$ were produced for wear protection in [3]. In regard to wear resistance, WC-Co and Cr_3C_2 -NiCr coatings were applied by APS, for example, in [4] and [5]. The APS WC-Co coating was superior to the conventional hard chromium electrodeposit in terms of wear resistance [4]. In addition to ceramic and carbide materials, APS is used to spray a wide range of metallic materials for various applications. In addition to typical materials such as Ni20Cr, MCrAlYs and various steels, novel metallic materials such as high-entropy alloys (HEA) can also be processed well with APS [6, 7]. The wear and oxidation behavior of HEA coatings was investigated in [6] and [7], respectively. Wear- and corrosion-resistant coatings are usually thinner than $d = 500 \mu m$, as shown in [2–7]. For applications such as part recovery, APS can also be used to deposit well adherent coatings thicker than $d = 1.5 mm$, as shown in [8]. The thick NiAl coatings could be turned to the desired dimension [8]. Due to the many process advantages, some of which are mentioned above, APS is also used to produce silicon coatings with powders of different size distributions [9–23]. A fine powder with a particle size distribution of $f = -45 + 1 \mu m$ was used to prepare the bond coat in EBC by Cojocar et al. [12], in which the performance of EBC exposed to thermal cycling in water vapor environment was investigated. A coarse powder of $f = -130 + 70 \mu m$ was used for the bond coats in [13], where the oxidation behavior of the bond coats was investigated. The influence of powder size distribution on the properties of APS coatings was studied by Niu et al. in [10]. He used three silicon powders of $f = -241 + 31 \mu m$, $f = -172 + 23 \mu m$ and $f = -68 + 9 \mu m$ to deposit coatings. Generally, compared to finer powders the silicon coatings prepared by coarser powders tend to have higher porosity [9–11]. The APS coating prepared with a silicon powder of $f = -50 + 10 \mu m$ had a porosity of $\Phi = 7.6\%$ in [9], while the APS coating deposited with the powder of $f = -172 + 23 \mu m$ had a porosity of more than $\Phi = 10\%$ in [10]. A finer silicon powder with an average size of $25.9 \mu m$ was used in [11], resulting in a lower porosity of $\Phi = 6.4\%$. With respect to EBC application, it is desirable to further reduce the porosity of APS silicon coatings and thus improve the oxidation behavior of the bond coat. In general, APS silicon coatings have relatively low oxide contents, as shown in [10]. The mass oxygen contents of the coatings in [10] are in the range of 0.64–1.19%. These values are at a low level for APS metallic coatings. The deposition efficiencies (DE) of silicon powders in amounts of $DE = 19$ – 20% are conventionally at

a low level for APS [10]. The microstructure and properties of APS silicon bond coat in EBCs are usually not the focus of publications which deal with EBCs. The silicon bond coat was investigated less in detail compared to the silicate top coats, as shown in [12–23]. Besides APS, vacuum plasma spraying (VPS) was also used to deposit silicon coatings [11, 24, 25]. The main process advantages of VPS over APS include the avoidance of interaction of feedstock materials with the ambient atmosphere, reduction of particle overheating and the possibility of cleaning the substrate. The main disadvantages compared to APS are the higher process costs and the limited sizes of the parts to be coated. The VPS silicon coatings present denser coating structures compared to APS silicon coatings. Porosity values of $\Phi = 1.1\%$, 1.19% and 3.2% are reported in [11, 24] and [25], respectively. Despite the denser structure of VPS coatings, APS is usually used instead of VPS for the deposition of silicon bond coats in EBCs because it is much cheaper compared to VPS. In addition to APS and VPS, silicon coatings can be prepared by flame spraying [26]. While coatings were produced using a reducing flame, no coatings could be prepared with a neutral flame [26]. The low DE values in [10] and the poor deposition behavior of the powder with a neutral flame in [26] are not explained in detail. Because the influence of spray parameters on the coating structure and the deposition efficiency of silicon powders has not been systematically investigated, this study was carried out to produce dense coatings by three-cathode plasma spraying. Furthermore, a better understanding of the reasons for the decreased deposition efficiencies of silicon powders can be gained. For this, the coatings were prepared under different spray conditions and the deposition efficiencies of the powder were determined. The particle in-flight properties were measured with aid of a particle diagnostic device to better understand the influence of parameters on the coating structure and the deposition efficiency of the powder. The coatings were investigated in terms of their surfaces and structures using electron scanning microscopy (SEM). The porosities of the coatings were optically determined. The results show that APS can be used to produce silicon coatings that can have similarly low porosities to VPS coatings when the appropriate parameters are used. Compared to the values reported in the literature, higher DE values were obtained in this study. The reasons for the low DE values of silicon powders are well explained.

2 Experiments

A commercially available silicon powder with a code SI006 delivered by the company Goodfellow GmbH, Hamburg, Germany, with a size distribution of $f = -53 + 15 \mu m$ was used as feedstock material. Figure 1 shows a backscattered electron (BSE) SEM micrograph of the silicon powder using

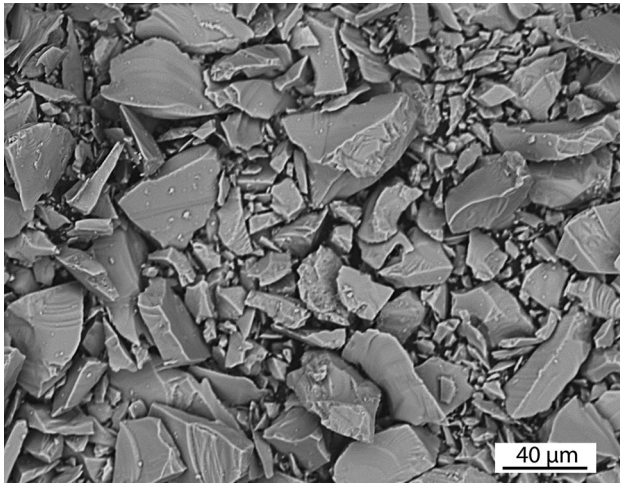


Fig. 1 Overview of the particle morphologies of the used silicon powder with a size distribution of $f = -53 + 15 \mu\text{m}$ imaged by BSE SEM

an apparatus PhenomX from the company Thermo Fisher Scientific, Eindhoven, The Netherlands. The silicon powder exhibited irregular particle morphologies due to its manufacturing process such as “melting and crushing”.

A three-cathode plasma generator TriplexProTM-210 from the company Oerlikon Metco Europe GmbH, Kelsterbach, Germany, was used to produce the coatings. Three-cathode plasma spraying generally provides a higher plasma stability compared to conventional one-cathode plasma spraying [27] and thus is advantageous for light materials like silicon. The spray parameters are given in Table 1.

The parameter set S-1 was selected for the production of the first coating, since dense titanium coatings can be produced with this parameter set. The high argon flow rate of $\dot{Q}_{\text{Ar}} = 100 \text{ SLPM}$ is used to reduce the oxidation of titanium particles. Because titanium has a melting point $T_m = 1,668 \text{ }^\circ\text{C}$, which is higher than that of silicon $T_m = 1,414 \text{ }^\circ\text{C}$, it was expected that dense and low-oxidation silicon coatings can be produced as well using this parameter set. The parameter sets S-2 to S-5 were chosen based on the previous test results to increase the melting degree of the powder. Compared to S-1, the electric power of the

plasma generator was increased to $P = 32.7 \text{ kW}$ by increasing the electric current to $I = 380 \text{ A}$ for S-2. In addition, the argon flow rate was decreased to $\dot{Q}_{\text{Ar}} = 70 \text{ SLPM}$ to enhance the dwell time of silicon particles in the plasma gas stream. Compared to S-2, the electric power of the plasma generator was increased to $P = 39.1 \text{ kW}$ by increasing the electric current to $I = 420 \text{ A}$ for S-3. Besides, the argon flow rate was decreased to $\dot{Q}_{\text{Ar}} = 60 \text{ SLPM}$ for S-3 to enhance the dwell time of silicon particles in the plasma gas stream compared to an argon flow rate of $\dot{Q}_{\text{Ar}} = 70 \text{ SLPM}$. Compared to S-3, the electric power of the plasma generator was increased to $P = 43.4 \text{ kW}$ by adding the secondary process gas hydrogen of $\dot{Q}_{\text{H}_2} = 2 \text{ SLPM}$ for S-4. In addition to the increased electric power, hydrogen improved the thermal conductivity of the plasma jet, thus heating silicon particles. Compared to S-4, the argon flow rate was reduced to $\dot{Q}_{\text{Ar}} = 50 \text{ SLPM}$ in S-5 to decrease the plasma gas velocity, thus increasing the dwell times of particles in the plasma gas stream. In this way, the melting degree of the powder should be further increased. The electric power slightly decreased to $P = 41.5 \text{ kW}$ due to the decreased argon flow rate. The parameter set S-6 was especially designed based on the result of S-5 to investigate the evaporation effect of the powder. The electric power of the plasma generator was intentionally increased to $P = 51.3 \text{ kW}$ to evaporate the silicon powder significantly more compared to S-5. Both a higher electric current of $I = 480 \text{ A}$ and a higher hydrogen flow rate of $\dot{Q}_{\text{H}_2} = 5 \text{ SLPM}$ were used in S-6. In order to observe the condensates on the front surface of the sample, the sample S-6 was coated only on its bottom half, which did not influence the comparison of the coating structure with other coatings.

The particle diagnostic system SprayWatch 4 s from the company Oseir Ltd., Tampere, Finland, was used to determine particles' in-flight velocities and temperatures at the used stand-off distance. The duration of a measurement was chosen to be $t = 2 \text{ min}$. to get sufficient particles which are identified as valid for the analysis program of SprayWatch 4 s. Carbon steel plates $L \times W \times H = 50 \times 40 \times 8 \text{ mm}^3$ were used as substrates. Shortly prior to coating, the steel samples were blasted with a white corundum powder F 20. The compressed air was set to $p = 4 \text{ bar}$ for blasting. The grit-blasting was finished after the dark scale on the steel samples was completely removed and a bright uniformly roughened surface appeared. The blasted samples were first cleaned with compressed air of $p = 6 \text{ bar}$ and then with ethanol, followed by coating with the plasma generator. The coated samples were cut and embedded for metallographic preparation. The porosities of the coatings were measured on their cross sections using an image analysis system from the company AxioVision, Carl Zeiss Jena GmbH, Jena, Germany. Since the porosity measurement with image analysis systems is based on setting the color contrast for pores and other coating components, the contrast setting significantly affects the measurement result. Many factors can influence the

Table 1 Spray parameter sets for TriplexProTM-210

Sample	Current (A)	Ar (SLPM)	H ₂ (SLPM)	Distance (mm)	Power (kW)
S-1	220	100	0	120	19.4
S-2	380	70	0	120	32.7
S-3	420	60	0	120	39.1
S-4	420	60	2	120	43.4
S-5	420	50	2	120	41.5
S-6	480	60	5	120	51.3

contrast setting, including pore size, coating materials, oxides in metallic coatings, image magnification, etc. In general, pores are black and oxides are colored with different tones of gray in metallic coatings. Metallic components are clearly brighter than pores and oxides. The contrast of pores to metallic components is easy to adjust. In comparison, the contrast of pores to oxides can be more difficult to adjust. Images with moderate magnifications up to $500\times$ provide a more reliable value for total porosity than images with high magnifications such as more than $2000\times$. The high-magnification images are more suitable for measuring fine pores in coatings. Since the total porosity of the coatings was determined in this study, some of the pores smaller than $\varnothing=2\ \mu\text{m}$ could not be measured. Since the silicon coatings had only low oxide contents, the influence of the oxides was limited. The DE of the powder was determined according to the Standard ISO 17836:2017. Carbon steel plates of $L \times W \times H=250 \times 250 \times 2\ \text{mm}^3$ were used as substrates for DE determination. The coatings were analyzed in terms of their surface topographies and coating structures using SEM.

After the coating process, the back side of the samples was documented by taking photographs of them with a high-resolution camera. The influence of process parameters can be compared by the amounts of condensates formed on the back side of the coated samples, which well indicate the melting degree and the evaporation degree of the powder. Dusts and condensates formed during spraying and adhered onto the coating surface as well. The dust on the coated sample for DE determination of S-4 and the condensates on the surface of sample S-6 were analyzed using SEM and energy-dispersive X-ray spectroscopy (EDS). The SEM analysis allowed to image the morphology of dust particles and to qualitatively investigate the local chemical composition of particles on the surface, as shown in [30]. For dust analysis, an adhesive tape, which is electrically conductive for SEM analysis, was first manually pressed onto the dust of the coated sample S-4 and then peeled off from the sample. The peeling was easy because the adhesion of the tape to the sample was poor due to the dust. Prior to SEM analysis, the dust was cleaned with 7 bar compressed air to remove poorly adhering particles from the tape. This was to avoid removing such particles when the vacuum was evacuated. The area with the most dust was selected for SEM analysis. There were a large number of dust particles in the selected area, allowing for a representative analysis result. The exact number of total particles was not counted.

3 Results and discussion

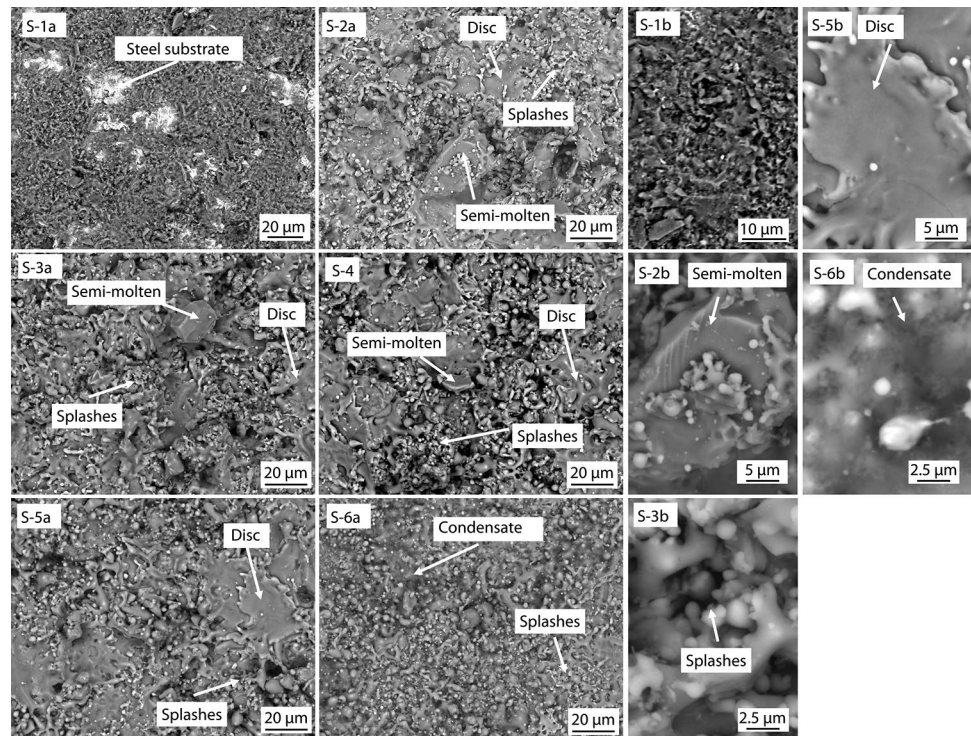
3.1 Particle temperatures and velocities

The average particle temperatures and average particle velocities for the parameter sets S-1 to S-6 were determined by SprayWatch 4 s. The measurement results are summarized in Table 2. The measurement did not give a valid result for S-1, since the silicon particles did not emit sufficient signals, which are needed for the analysis program. Most of the silicon particles were not sufficiently heated, since silicon particles were shortly accelerated to high velocities due to the high argon flow rate of $\dot{Q}_{\text{Ar}}=100\ \text{SLPM}$ and the low density of silicon $\rho_{\text{Si}}=2.33\ \text{g/cm}^3$. In contrast to S-1, a particle temperature of $T_p=2,700 \pm 33\ ^\circ\text{C}$ was determined for S-2, which is higher than the boiling point $T_b=2,355\ ^\circ\text{C}$ of silicon. Attention must be paid to the fact that the measured particle temperature was based on the surface temperature of particles. Because the determined value is higher than the boiling point of silicon, it is reasonable to state that the evaporation of silicon particles occurred on surfaces of some silicon particles. The signals emitted from the particle surfaces and their near-surface vapor products together influenced the measured particle temperature. The particle velocity for S-2 was measured to be $v_p=269 \pm 2\ \text{m/s}$. Both the particle temperature and velocity values are at high levels for common APS processes. A particle temperature of $T_p=2,650 \pm 20\ ^\circ\text{C}$ and particle velocity of $v_p=271 \pm 3\ \text{m/s}$ were determined for S-3. Both values are similar to those of S-2. Compared to S-2, the increased electric powder of the plasma generator influenced positively the particle velocity due to increasing plasma gas velocity. The decreased argon flow rate influenced negatively the particle velocity due to decreasing gas flow impulse. Both effects compensated, resulting in the similar particle velocity to that of S-2. In contrast to the particle velocity, the similarity in particle temperature is difficult to explain. One possible reason could be that the evaporation of silicon particles influenced significantly the measurement. In addition, the error of particle temperature measurement is in a range of 5–10% based on the measuring principle [28]. The real particle temperatures of S-2 and S-3 could differ more than the measured values. A particle temperature of $T_p=2,690 \pm 20\ ^\circ\text{C}$ and a particle velocity of $v_p=298 \pm 13\ \text{m/s}$ were measured for S-4. The increased particle velocity was attributed to the increased electric power as above mentioned. The temperature value is also similar to those of S-2 and S-3. The similarity in the particle temperature

Table 2 Average particle temperatures and velocities determined by SprayWatch 4 s

	S-1	S-2	S-3	S-4	S-5	S-6
$T_p\ (^{\circ}\text{C})$	Not valid	$2,700 \pm 33$	$2,650 \pm 20$	$2,690 \pm 20$	$2,700 \pm 25\ ^{\circ}\text{C}$	$3,390 \pm 92$
$v_p\ (\text{m/s})$	Not valid	269 ± 32	271 ± 3	298 ± 13	277 ± 40	360 ± 20

Fig. 2 BSE SEM micrographs of the surfaces of the APS-sprayed silicon coatings S-1 to S-6



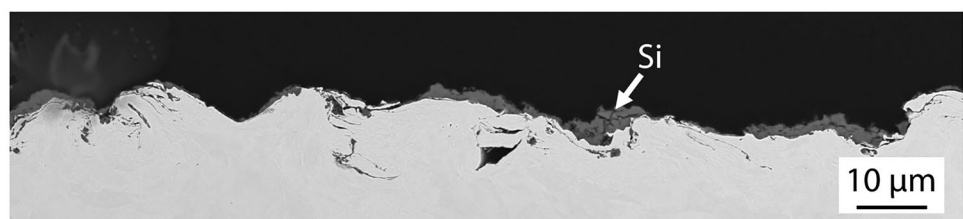
is seen for S-5 with $T_p = 2,700 \pm 25$ °C. As expected, the particle velocity decreased $v_p = 277 \pm 40$ m/s for S-5 compared to S-4 due to the decreased argon flow rate. A significantly higher particle temperature and particle velocity of $T_p = 3,390 \pm 92$ °C and $v_p = 360 \pm 20$ m/s were measured for S-6 due to its significantly higher electric powder and higher hydrogen flow rate of S-6 compared to the other parameter sets. Summarily, the measurement results show that all parameter sets led to high particle velocities due to the low density of silicon. High particle temperatures were determined for the parameter sets S-2 to S-6. However, the influence of the parameter sets could not be recognized for the parameter sets S-2 to S-5.

3.2 Surface morphologies, coatings structures and DE values

Coating S-1: Figure 2 shows BSE-SEM micrographs of the surfaces of coatings S-1 to S-6. While Fig. 2 (S-1a) to (S-6a) provide an overview of the characteristics of the

surfaces of coatings, the special sites marked in (S-1a) to (S-6a) can be observed under higher magnifications in Fig. 2 (S-1b), (S-2b), (S-3b), (S-5b), and (S-6b). As shown in Fig. 2 (S-1a), the light areas are the steel substrate and the dark areas are the silicon coating. The steel substrate is not completely covered by the coating, which shows the coating is extremely thin. The coating surface can be seen in more detail in Fig. 2 (S-1b). The surface topography shows the typical characteristic of a brittle broken surface, which is depicted by the angular shapes of splats. Solid silicon particles in plasma gas stream can remain relatively hard and abrasive as reported in [31]. They eroded the formed coating due to their high velocities, leading to the brittle broken surface feature. Figure 3 presents a BSE SEM micrograph of a cross section of coating S-1, confirming that the substrate is not completely covered by the very thin coating. The coating consists of fine lamellae. The fine lamellae are damaged in the marked area. The fine lamellae indicate that some

Fig. 3 A BSE SEM micrograph of a cross section of the APS-sprayed silicon coating S-1 with DE = 1.5%



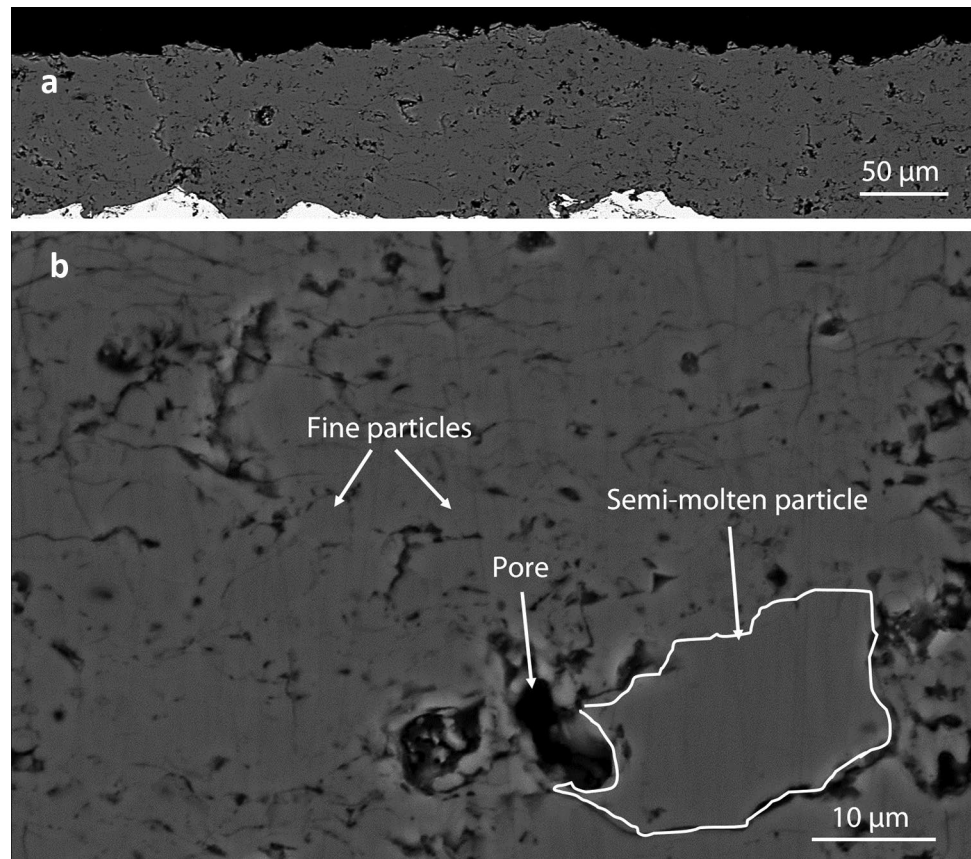
of the smaller particles in the powder were melted. Semi-molten particles, as seen in the following coatings S2 to S6, are not visible in this coating, indicating that the solid cores of semi-molten particles bounced off when they hit the substrate. The DE was determined to be only $DE = 1.5\%$. The reason for the very low DE was that the silicon particles were not sufficiently heated, resulting in a very low melting degree of the powder. The parameter set S-1 is selected since it can be used to produce dense titanium coatings using titanium powders with a size distribution $f = -63 + 11 \mu\text{m}$ or $f = -45 + 11 \mu\text{m}$. Compared to the titanium powders, the dwell times of silicon particles in the plasma gas stream were significantly shorter due to its significantly lower density compared to that of titanium. Accordingly, there were a large number of abrasive unmolten particles and big solid cores of semi-molten particles.

Coating S-2: A BSE SEM micrograph of the surface of coating S-2 is also shown in Fig. 2. The surface features of coating S-1 are no longer visible. This shows that the grit-blasting effect significantly decreased compared to S-1. This indicates that the silicon particles were more melted compared to S-1. The topography of S-2 is characterized by disc-like splats, a large number of fine particles and semi-molten particles. Since the disc-like splats and fine particles are similar for coatings S-2 to S-6, a disc-like splat is exemplified in Fig. 2 (S-5b) and the fine particles in Fig. 2 (S-3b). It is well known that disc-like splats result from melted particles with suitable velocities. The disc-like splats on the surface S-2a are typically smaller than $\varnothing = 30 \mu\text{m}$, indicating that they formed from small melted silicon particles. The fine particles as shown in Fig. 2 (S-3b) formed from splashed silicon melt. It is known that semi-molten metallic and ceramic particles generally splash upon impact with a substrate due to their solid cores. In addition, melted silicon particles also splashed when their velocities were too high for the formation of disc-like splats. In general, high particle velocities and low viscosities of silicon melt favor splashing of melted silicon particles [9]. The semi-molten particle as seen in Fig. 2 (S-2b) shows an irregular form as silicon particles in Fig. 1. The surface characteristic of original silicon particles is partly recognizable, indicating that this particle hardly melted in the marked area. It can be seen that the molten part of this semi-molten particle came into contact with its underlying coating area. This shows that if the molten part of a semi-molten particle is large enough and comes into contact with the substrate upon impact, the molten part can hinder the solid core from bouncing off, allowing the solid core to adhere. The larger the molten

portion of a semi-molten particle, the more likely it is to adhere. Figure 4a, b presents two BSE SEM micrographs of a cross section of coating S-2, giving an overview and details of the coating structure. The overview reveals a relatively homogenous but porous structure. The porosity was measured to be approximately $\Phi = 15\%$. The coating mainly exhibited lamellae and particles. The boundaries of particles are partly smooth, indicating that they were most likely solid parts of semi-molten particles. Besides, pores and relatively big semi-molten particles are recognizable. The semi-molten particles indicate the insufficient heating of numerous particles in the plasma gas stream. The high porosity should mainly be caused by the numerous semi-molten particles as well, as they could not sufficiently flatten when reaching the substrate. The determined DE value amounts to $DE = 18.7\%$, being significantly higher compared to S-1 and similar to those values reported in [10] for conventional one-cathode plasma spraying. Two influencing factors were important for the relatively low DE value. One was that there were still numerous semi-molten particles, which especially with bigger solid parts easily bounced off as their impacting the substrate during the spraying process. Another one was the splashing of melted and semi-molten particles, which led to loss of silicon melt to the surrounding atmosphere.

Coating S-3: A BSE SEM image of the surface of coating S-3 is presented in Fig. 2 as well. In general, the surface of coating S-3 looks like that of coating S-2. The topography of S-3 is again characterized by disk-like splats, a large number of fine particles and semi-molten particles. The marked semi-molten particle is smaller than the marked semi-molten particle on the surface of coating S-2. Figure 5a, b presents two BSE SEM micrographs of a cross section of coating S-3. The overview reveals a denser structure compared to S-2. The porosity was measured to be approximately $\Phi = 4.5\%$. This value is lower than the values reported in the literature. In addition, it can be seen that some of lamellae in coating S-3 are larger than those in coating S-2. The increased power of the plasma generator and the reduction in argon flow rate resulted in a higher melting degree of the powder compared to S-2. Accordingly, the influence of the semi-molten particles on pore formation decreased due to the reduced number of semi-molten particles and smaller solid cores of the semi-molten particles. In addition, the percentage of larger particles in the powder that were melted increased compared to S-2. The melted larger particles resulted in the larger lamellae. The determined DE value increases to $DE = 24.1\%$. Due to the enhanced melting degree of the powder, the material loss by bouncing-off of semi-molten

Fig. 4 BSE SEM micrographs of a cross section of the APS-sprayed silicon coating S-2 with $\Phi = 15\%$ and $DE = 18.7\%$: fine particles, pore and semi-molten particle are marked in (b)



particles decreased compared to S-2, too. In contrast, it was possible for melted and semi-molten particles to splash increasingly.

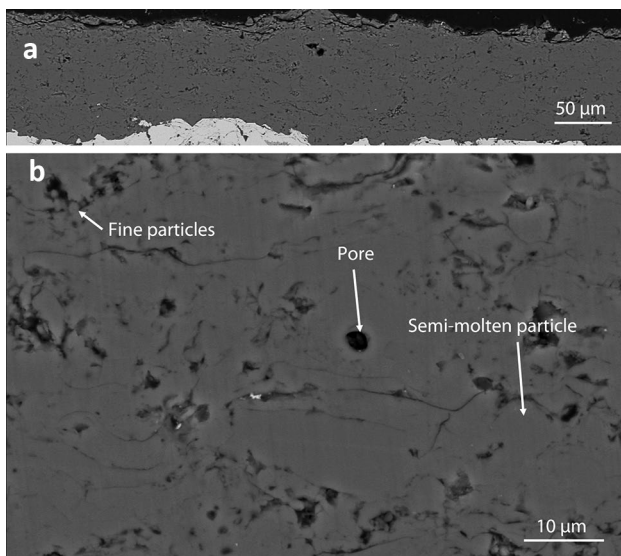


Fig. 5 BSE SEM micrographs of a cross section of the APS-sprayed silicon coating S-3 with $\Phi = 4.5\%$ and $DE = 24.1\%$: fine particles, pore and semi-molten particle are marked in (b)

Coating S-4: A BSE SEM micrograph of the surface of coating S-4 is shown in Fig. 2 as well. The topography of S-4 is characterized by disk-like splats, a large number of fine particles and semi-molten particles as well. The marked semi-molten particle is significantly smaller than the marked one on the surface of coating S-2. The addition of hydrogen as a secondary plasma gas not only increased the power of the plasma generator, but also the thermal conductivity of the plasma gas stream. This further improved the melting degree of the powder compared to S-3. Despite this improved melting degree, numerous particles were still semi-molten due to the short heating times. Figure 6a, b presents two BSE SEM micrographs of a cross section of coating S-4. The overview of the coating shows a dense and homogenous structure. Some of the semi-molten particles look cleaner and smoother than the adjacent areas as shown in Fig. 6b. The reason for this could be that the adjacent areas had more structural defects such as pores and boundary gaps. The porosity was measured to be $\Phi = 2\%$, being lower compared to S-3 as well as those of the coatings in [10]. This porosity value is already within the range of VPS coatings as reported in the literature, showing that dense coatings can also be produced with APS if the appropriate parameters are used. The increased melting degree of the

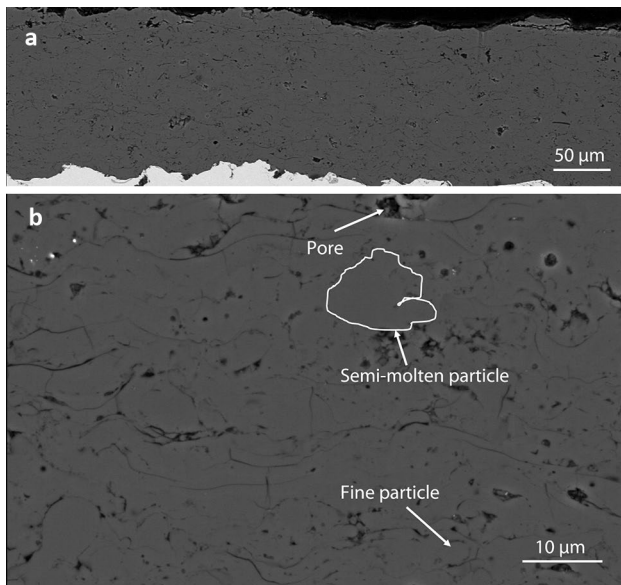


Fig. 6 BSE SEM micrographs of a cross section of the APS-sprayed silicon coating S-4 with $\Phi=2\%$ and $DE=28\%$: fine particles and semi-molten particle are marked in (b)

powder led to a better flattening of particles. The DE was determined to be $DE=28\%$, being more than 40% higher compared to S-2 and those values found in the literature [10]. On the one hand, the loss of silicon due to the bouncing of solid cores of semi-molten particles decreased compared to S-3. On the other hand, the splashing of silicon melt increased compared to S-3. The reduction in loss of solid cores of semi-molten particles was greater than the increased loss of silicon due to splashing, resulting in the higher DE for S-4.

Coating S-5: A BSE SEM micrograph of the surface of coating S-5 is also seen in Fig. 2. Disk-like splats and a large number of fine particles are recognizable. Big semi-molten particles like that on the surface of S-2 are not visible. Figure 7a, b presents two BSE SEM micrographs of a cross section of coating S-5. The overview of the coating shows a homogenous structure. The coating was more porous compared to S-4. The porosity was measured to be approximately $\Phi=10\%$. In Fig. 7b, a pore is marked that consists of very fine particles. Such areas in the coating were evaluated as pores by the image analysis program. Therefore, the actual porosity of coating S-5 must be lower than this determined value. In addition, more fine particles are seen in coating S-5 than in coating S-4, indicating that semi-molten particles and melted particles splashed more compared to S-4. The increased splashing resulted from the improved

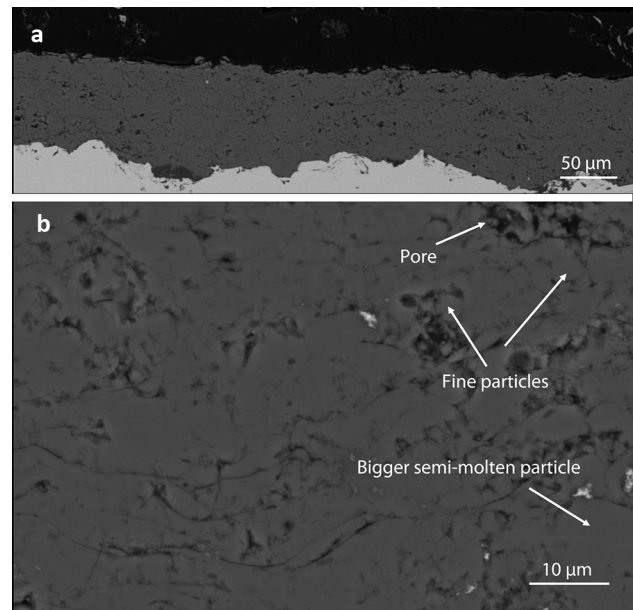


Fig. 7 BSE SEM micrographs of a cross section of the APS-sprayed silicon coating S-5 with $\Phi=10\%$ and $DE=25.1\%$: fine particles, pore and semi-molten particle are marked in (b)

melting degree of the powder compared to S-4. The higher melting degree of the powder was due to the lower argon flow rate which increased the heating times of the silicon particles in the plasma gas stream. The higher porosity of coating S-5 compared to S-4 shows that the coating porosity cannot be linearly correlated with the melting degree of the powder. One possible reason for the higher porosity despite the higher melting degree could be that the increased splashing caused the formation of significantly more clusters of fine particles, which could hinder the flattening of melted silicon particles. Another possible reason was that the evaporation of silicon particles increased and more condensates formed accordingly. The condensates could hinder the adhesion and flattening of silicon melt and promote pore formation. This evaporation effect is more pronounced in coating S-6, as will be shown below. These two factors resulted in the higher porosity despite the reduced number of semi-molten particles and the smaller sizes of their solid cores. Figure 7b shows fewer semi-molten particles that are clearer and smoother than the adjacent areas compared to S-4. This is due to the fact that the adjacent areas with structural defects are generally larger compared to S4. The DE was determined to be $DE=25.3\%$, being less than that of S-4 despite an improved melting degree of the powder. The reason for this was the increased splashing and evaporation

effect, too. Besides material loss caused by evaporation, the condensates on the coating surface between single passes could obstruct the contact and spread of particles during flattening on the substrate. Locations with high amounts of condensates had to be cleaned through the impacts of following particles to provide a suitable surface quality for flattening. As a result, more particles splashed or bounced off. Therefore, the total silicon loss increased due to the effects of splashing and evaporation, although the loss of solid cores of semi-molten particles decreased compared to S-4.

Coating S-6: A BSE SEM micrograph of the surface of coating S-6 is also presented in Fig. 2, which significantly differs from those of other coatings. In addition to a large number of fine particles, numerous condensates can also be seen, as shown in Fig. 2 (S-6b). The condensates are darker than elsewhere because the condensates are oxides, as shown in more detail in Fig. 10. Figure 8 shows two BSE SEM micrographs of coating S-6. While oxides in coatings S-2 to S-5 are barely recognizable on their cross sections, oxides are clearly visible in Fig. 8b. As mentioned in the introduction, APS silicon coatings generally have relatively low oxygen contents. This is also valid for coatings S-2 to S-5. This shows that the oxidation of silicon was limited both in flight and during impact and cooling for S-2 to S-5. The reason for the low degree of oxidation in flight could be due to the evaporation of melted and semi-molten silicon particles, which hindered the transport of atmospheric oxygen to the particle surfaces. The low degree of oxidation on the substrate can be explained by the barrier effect of thermally grown oxide SiO_2 . When a very thin, adherent SiO_2 film formed on solidified lamellae or semi-molten particles, the growth of SiO_2 is very slow [13]. Compared to coatings S-2 to

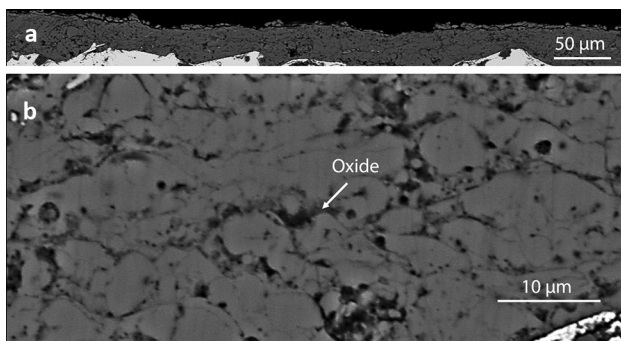


Fig. 8 BSE SEM micrographs of a cross section of the APS-sprayed silicon coating S-6 with $\Phi=9.0\%$ and $DE=11.1\%$: oxides are marked in (b)

S-5, the silicon particles evaporated significantly more and large amounts of condensates were formed as oxides, as shown in Fig. 10. Some of the condensates were removed by the subsequent impacting particles and some of them were trapped in the coating. This was the main reason for the higher oxide content of coating S-6. The strong evaporation of the silicon particles also favored the formation of pores, as already discussed for S-5. The porosity was measured to be $\Phi=9.0\%$ despite the highest particle velocity. This coating is significantly thinner than coatings S-2 to S-5 due to the strong evaporation. A DE value of $DE=11.1\%$ was determined. The evaporation of the powder and the condensates were further analyzed in the following subchapter.

3.3 Analysis of the condensate and dusts

Figure 9 shows pictures of the back sides of the coated sample S-1 to S-5. Condensates are not clearly visible on the backs of samples S-1 and S-2. In contrast, condensates are visible on the back side of S-3. Silicon easily evaporates at high temperatures [29]. Because the gas stream had turbulent flows when it impacted the substrate, some species in the gas stream could contact the back side of the sample. As a result, the silicon vapor or oxidized silicon vapor (gaseous silicon oxide) in the gas stream partly condensed on the back side of the sample. The amounts of condensates depended on the concentration of evaporated silicon in the plasma gas stream. For S-1 and S-2, the amounts of evaporated silicon in the plasma gas stream were so low that the condensates on their back-sides were not as clearly visible as on the backsides of the other coatings. This again shows that parameter sets S-1 and S-2 resulted in lower melting degrees and evaporation of the powder compared to parameter sets S-3 to S-6. The amounts of condensates increased from S-3 to S-5, indicating that the silicon powder was subsequently more heated, melted and evaporated. The variation of the parameters improved the melting degree of the powder as expected and increased the evaporation of the powder as well.

The pictures of the coating surface and the back side of sample S-6 are presented in Fig. 9 as well. As expected, significantly more condensates are recognizable both on the upper half of the front side and the back side of the sample compared to the other samples. Figure 10 shows a BSE SEM micrograph of the white condensate on the front side. The result of the EDS area-measurement on this surface area is also shown in Fig. 10. The mass content of silicon and oxygen (O) is 45.79% and 54.03%,

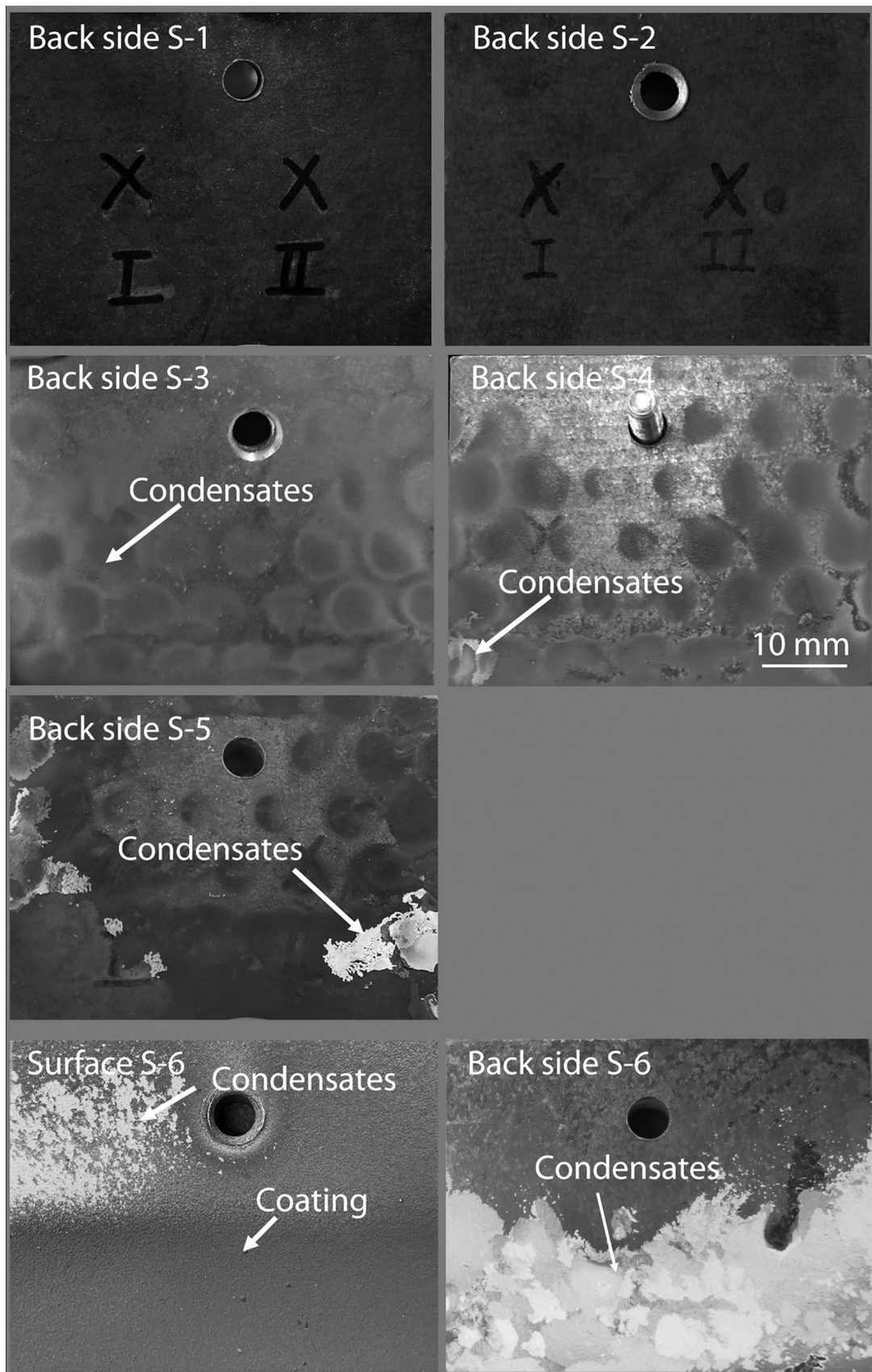


Fig. 9 Pictures of the back sides of the coated samples S-1 to S-6 and a picture of the front side of the coated sample S-6

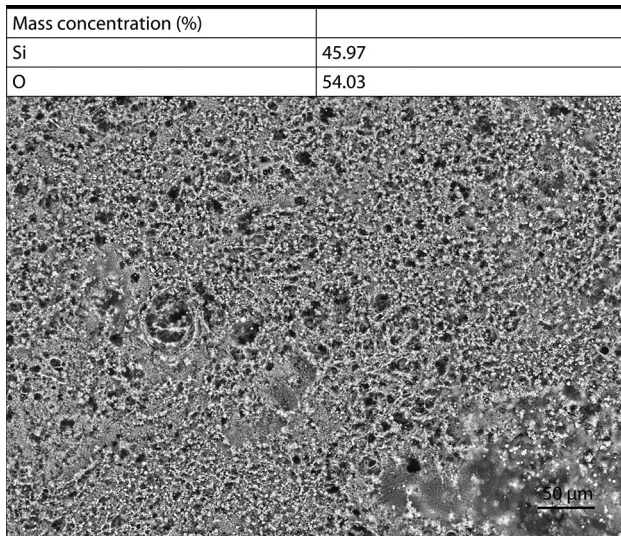


Fig. 10 A BSC SEM micrograph of the white condensates on the front upper side of sample S-6 and the qualitative result of EDS area-measurement on it

respectively. In addition to this surface area, two other surfaces were measured, resulting in 54.50% O and 45.50% Si, and 52.14% O and 47.86% Si. The average mass contents of oxygen and silicon are $53.56 \pm 1.25\%$ and $46.44 \pm 1.25\%$, respectively. No fine particles and no semi-molten particles are recognizable in the condensates. The EDS result shows that the whole area consisted qualitatively of silicon oxide.

There were dusts on the surfaces of the coated samples for DE determination. Figure 11 shows a BSE SEM micrograph of the transferred dust on the tape from the surface of sample S-4. It is recognizable that the dust consisted mainly

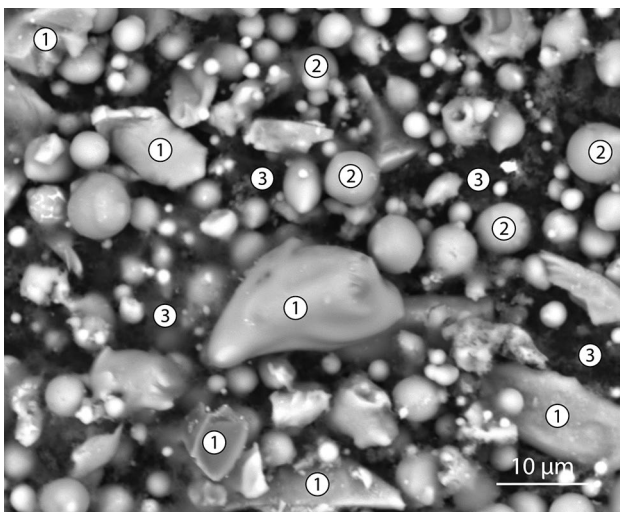


Fig. 11 A BSE SEM micrograph of the dusts from the sample for DE determination S-4

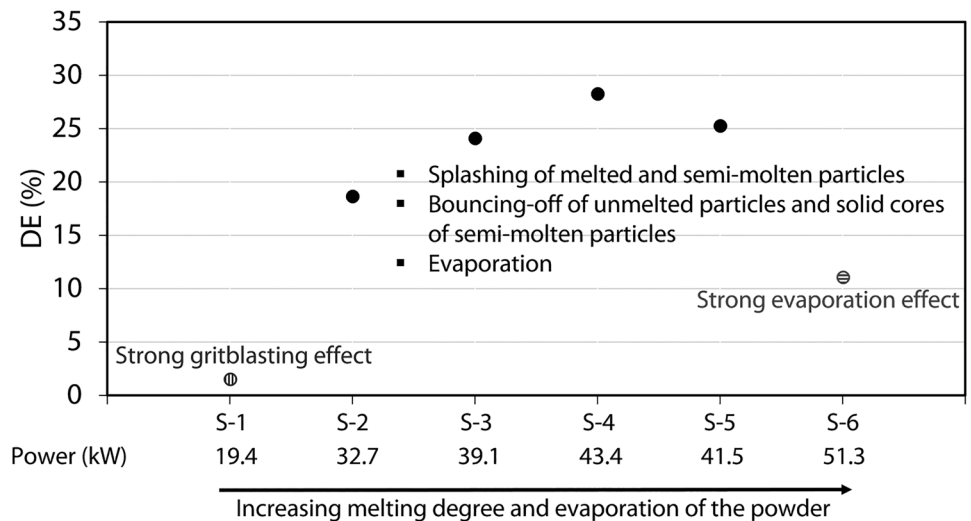
of three components: irregular particles like the one marked with “1,” spherical smooth particles like the one marked with “2” and gray matrix like the one marked with “3”. Most of spherical particles were a few micrometers small. The spherical particles formed from the splashed silicon melt. Liquid splashes solidified in-flight into fine spheric particles. Some of them exhibited a sufficient adhesion to the surface. Another reason for fine spheric particles could be that small melted or semi-molten particles already solidified before they impacted the substrate. The smoother surfaces of irregular particles compared to those of original particles reveal that they were solid parts of semi-molten particles. The bounced-off solid cores of semi-molten particles were included in the dust. The morphologies of the gray matrix indicate that they were condensates from evaporated silicon or oxidized silicon vapor.

3.4 Discussion on the main influencing factors for DE

The influence of the spray parameters on the DE value of the silicon powder is summarized in Fig. 12. It can be seen that the strong grit-blasting effect was the main reason for the lowest DE value of S-1. On the other side, the strong evaporation effect was the main reason for the second lowest DE value of S-6. The DE values of S-2 to S-5 are significantly higher than those of S1 and S-6. The DE value increases from S-2 to S-4 due to the increasing melting degree of the powder. The splashing of melted and semi-molten particles and the bouncing-off of solid cores of semi-molten particles were mainly responsible for material losses for S-2 to S-5. In addition, the evaporation of silicon particles was recognizable for S-3, S-4 and S-5. The evaporation of silicon particles caused material losses, too. Its contribution to the low DE values should be less than those by the above-mentioned two factors.

Based on the results of this study, it could be assumed that the poor deposition behavior of the powder using a neutral flame in [26] could be due to a strong evaporation effect, since the powder was heated much more compared to the reducing flame [26]. The condensates of evaporated silicon in the neutral flame could hinder the adhesion of particles in some places, since the cleaning effect of following particles was not sufficient to remove the condensates sufficiently due to their significantly lower velocities compared to the particle velocities in this study. As a result, a complete covering coating was not formed. The low DE values in [10] should be mainly due to the same influencing factors as in cases of S-2 to S-5. Among them, semi-molten particles should play the most important role, since the powders used in [10] were coarser compared to the powder used in this study. In general, the low DE values of silicon powders in different spraying processes can be well explained with the help of Fig. 12.

Fig. 12 DE values of the APS-sprayed silicon coatings S-1 to S-6 with the main influencing factors for DE



4 Conclusions and outlook

In this study, the influence of spray parameters on the coating structure and the deposition efficiency of a silicon powder $f = -53 + 15 \mu\text{m}$ by three-cathode plasma spraying was investigated. The conclusions are summarized in the following:

1. There is a nonlinear correlation between the spray parameters and the DE.
2. A suitable melting degree of the powder like that of parameter set S-4 is important for a dense coating structure and a higher DE value. A very low melting degree of the powder like that of parameter set S-1 leads to a strong grit-blasting effect. In contrast, a high melting degree of the powder is accompanied by a strong evaporation effect as in case of parameter set S-6. Both decrease strongly the DE value.
3. Due to the low density of silicon, silicon particles are shortly accelerated to high velocities. Correspondingly, semi-molten particles always exist in particle jets during APS process despite various spray parameters. The splashing of melted and semi-molten particles and the bouncing-off of solid cores of semi-molten particles are the most important factors for the DE value in a wide range of spray parameters. These lead to generally low DE values in this study and in the literature.

Suitable parameter sets for the production of dense silicon coatings were determined in this study. Based on the results of this study, dense free-standing silicon coatings will be fabricated in the future. The free-standing coatings will be subjected to various oxidation tests to investigate their oxidation behavior and the structural influence on their oxidation behavior.

Acknowledgements The authors would like to thank the German Science Foundation (DFG) for financially supporting the research work within the scope of DFG project BO1979/73-1 (Project number: 428973451).

Funding Open Access funding enabled and organized by Projekt DEAL. The research work was financially supported by DFG (Deutsche Forschungsgemeinschaft) within the scope of DFG project BO1979/73-1 (Project number: 428973451).

Availability of data and materials Not applicable.

Code availability Not applicable.

Declarations

Ethics approval Not applicable.

Consent to participate Not applicable.

Consent for publication Not applicable.

Conflicts of interest The authors have no relevant financial or non-financial interests to disclose.

Open Access This article is licensed under a Creative Commons Attribution 4.0 International License, which permits use, sharing, adaptation, distribution and reproduction in any medium or format, as long as you give appropriate credit to the original author(s) and the source, provide a link to the Creative Commons licence, and indicate if changes were made. The images or other third party material in this article are included in the article's Creative Commons licence, unless indicated otherwise in a credit line to the material. If material is not included in the article's Creative Commons licence and your intended use is not permitted by statutory regulation or exceeds the permitted use, you will need to obtain permission directly from the copyright holder. To view a copy of this licence, visit <http://creativecommons.org/licenses/by/4.0/>.

References

- Lee KN, Zhu D, Lima RS (2021) Perspectives on environmental barrier coatings (EBCs) manufactured via air plasma spray (APS) on ceramic matrix composites (CMCs): a tutorial paper (2021). *J Therm Spray Technol* 30:40–58. <https://doi.org/10.1007/s11666-021-01168-0>
- Bobzin K, Zhao L, Öte M, Königstein T (2019) A highly porous thermal barrier coating based on Gd_2O_3 - Yb_2O_3 co-doped YSZ. *Surf Coat Technol* 366:349–354. <https://doi.org/10.1016/j.surfcoat.2019.03.064>
- Abdel-Samad AA, Bahloul AMM, Lugscheider E, Rassoul SA (2000) A comparative study on thermally sprayed alumina based ceramic coatings. *J Mater Sci* 35:3127–3130. <https://doi.org/10.1023/A:1004824104162>
- Sohi MH, Ghadami F (2010) Comparative tribological study of air plasma sprayed WC-12%Co coating versus conventional hard chromium electrodeposit. *Tribol Int* 43:882–886. <https://doi.org/10.1016/j.triboint.2009.12.049>
- Dzhurinskiy D, Babu A, Pathak P, Elkin A, Dautov S, Shornikov P (2021) Microstructure and wear properties of atmospheric plasma-sprayed Cr_3C_2 -NiCr composite coatings. *Surf Coat Technol*. <https://doi.org/10.1016/j.surfcoat.2021.127904>
- Ghadami F, Ghadami S, Davoudabadi MA (2022) Sliding wear behavior of the nanoceria-doped AlCrFeCoNi high-entropy alloy coatings deposited by air plasma spraying technique. *J Therm Spray Technol* 31:1263–1275. <https://doi.org/10.1007/s11666-022-01354-8>
- Ghadami F, Davoudabadi MA, Ghadami S (2022) Cyclic oxidation properties of the nanocrystalline AlCrFeCoNi high-entropy alloy coatings applied by the atmospheric plasma spraying technique. *Coatings*. <https://doi.org/10.3390/coatings12030372>
- de Lacalle LLN, Gutierrez A, Lamikiz A, Fernandes MH, Sanchez JA (2001) Turning of thick thermal spray coatings. *J Therm Spray Technol* 31:1263–1275, 10:249–254
- Niu Y, Liu X, Ding C (2006) Phase composition and microstructure of silicon coatings deposited by air plasma spraying. *Surf Coat Technol* 201:1660–1665. <https://doi.org/10.1016/j.surfcoat.2006.02.040>
- Niu Y, Zheng X, Liu X, Ji H, Ding C (2012) Influence of powder size on characteristics of air plasma sprayed silicon coatings. *Ceram Int* 38:5897–5905. <https://doi.org/10.1016/j.ceramint.2012.03.080>
- Niu Y, Liu X, Ding C (2006) Comparison of silicon coatings deposited by vacuum plasma spraying (VPS) & atmospheric plasma spraying (APS). *Mater Sci Forum* 510–511:802–805. <https://doi.org/10.4028/www.scientific.net/MSF.510-511.802>
- Cojocar CV, Kruger SE, Moreau C, Lima RS (2011) Elastic modulus evolution and behavior of Si/Mullite/BSAS-based environmental barrier coatings exposed to high temperature in water vapor environment. *J Therm Spray Technol* 20:92–99. <https://doi.org/10.1007/s11666-010-9599-4>
- Lee KN (2019) $Yb_2S_2O_7$ environmental barrier coatings with reduced bond coat oxidation rates via chemical modifications for long life. *J Am Ceram Soc* 102:507–1521. <https://doi.org/10.1111/jace.15978>
- Harder RJ, Almer JD, Weyant CM, Lee KN, Faber KT (2009) Residual stress analysis of multilayer environmental barrier coatings. *J Am Ceram Soc* 92:452–459. <https://doi.org/10.1111/j.1551-2916.2008.02888.x>
- Arai Y, Sato M, Kagawa Y (2018) Melting/Solidification of Si bond coat layer in oxide/Si/RB-SiC environmental barrier coating system. *Adv Eng Mater*. <https://doi.org/10.1002/adem.201800677>
- Xiao J, Liu Q, Li J, Guo H, Xu H (2019) Microstructure and high-temperature oxidation behavior of plasma-sprayed Si/ Yb_2SiO_5 environmental barrier coatings. *Chin J Aeronaut* 32:1994–1999. <https://doi.org/10.1016/j.cja.2018.09.004>
- Klemm H, Schönfeld K, Kunz W (2020) Delayed formation of thermally grown oxide in environmental barrier coatings for non-oxide ceramic matrix composites. *Coatings*. <https://doi.org/10.3390/coatings10010006>
- Kane KA, Garcia E, Uwanyuze S, Lance M, Unocic KA, Sampath S, Pint BA (2020) Steam oxidation of ytterbium disilicate environmental barrier coatings with and without a silicon bond coat. *J Am Ceram Soc*. <https://doi.org/10.1111/jace.17650>
- Arai Y, Inoue R, Kakisawa H (2021) Anisotropic crack propagation behavior for the silicon-bond coat layer in a multilayer coated system. *Int J Appl Ceram Technol* 18:947–956. <https://doi.org/10.1111/ijac.13679>
- Kedir N, Garcia E, Kirk C, Gao J, Guo Z, Zhai X, Sun T, Fezzaa K, Sampath S, Chen W (2021) Impact damage of narrow silicon carbide (SiC) ceramics with and without environmental barrier coatings (EBCs) by various foreign object debris (FOD) simulants. *Surf Coat Technol*. <https://doi.org/10.1016/j.surfcoat.2020.126779>
- Deijkers JA, Wadley HNG (2021) A duplex bond coat approach to environmental barrier coating systems. *Acta Mater*. <https://doi.org/10.1016/j.actamat.2021.117167>
- Bakan E, Marcano D, Zhou DP, Sohn YJ, Mauer G, Vassen R (2017) $Yb_2Si_2O_7$ environmental barrier coatings deposited by various thermal spray techniques: a preliminary comparative study. *J Therm Spray Technol* 26:1011–1024. <https://doi.org/10.1007/s11666-017-0574-1>
- Vassen R, Bakan E, Sebold D, Sohn YJ (2021) Correlation of process conditions, porosity levels and crystallinity in atmospherically plasma sprayed $Yb_2Si_2O_7$ environmental barrier coatings. *J Compos Sci*. <https://doi.org/10.3390/jcs5080198>
- Varacalle DJ, Herman H, Bancke GA, Burchell TD, Romannoski GR (1991) Vacuum-plasma-sprayed silicon coatings. *Surf Coat Technol* 49:24–30. [https://doi.org/10.1016/0257-8972\(91\)90026-S](https://doi.org/10.1016/0257-8972(91)90026-S)
- Niu Y, Liu X, Ding C (2008) Vacuum-plasma-sprayed silicon coatings for biomedical application. *Mater Sci Eng* 28:1132–1137. <https://doi.org/10.1016/j.msec.2007.07.001>
- Nistal A, García E, García-Diego C, Osendi MI, Miranzo P (2015) Flame spraying of adherent silicon coatings on SiC substrates. *Surf Coat Technol* 270:8–15. <https://doi.org/10.1016/j.surfcoat.2015.03.025>
- Bobzin K, Öte M, Schein J, Zimmermann S, Mohwald K, Lummer C (2016) Modelling the plasma jet in multi-arc plasma spraying. *J Therm Spray Technol* 25:1111–1126. <https://doi.org/10.1007/s11666-016-0438-0>
- Fincke JR, Haggard DC, Swank WD (2001) Particle temperature measurement in the thermal spray process. *J Therm Spray Technol* 10:255–266. <https://doi.org/10.1361/105996301770349358>
- Davis SG, Anthrop DF, Searcy AW (1961) Vapor pressure of silicon and the dissociation pressure of silicon carbide. *J Chem Phys* 34:659–664. <https://doi.org/10.1063/1.1701004>
- Gorji NE, Connor RO, Brabazon D (2021) XPS, SEM, AFM, and Nano-Indentation characterization for powder recycling within additive manufacturing process. *IOP Conf Ser Mater Sci Eng* 1182:012025. <https://doi.org/10.1088/1757-899X/1182/1/012025>
- Ingham HS, Shepard AP (1965) Flame spray handbook, Volume III Plasma Flame Process, METCO Inc., New York, ASIN: B004113WLI

Publisher's Note Springer Nature remains neutral with regard to jurisdictional claims in published maps and institutional affiliations.